ELSEVIER

Chemical Geology 242 (2007) 351–370

CHEMICAL GEOLOGY
INCLUDING
ISOTOPE GEOSCIENCE

www.elsevier.com/locate/chemgeo

Reliable extraction of a deepwater trace metal isotope signal from Fe–Mn oxyhydroxide coatings of marine sediments

Marcus Gutjahr [a,*], Martin Frank [a,1], Claudine H. Stirling [a,2], Veronika Klemm [a], Tina van de Flierdt [b], Alex N. Halliday [c]

[a] *ETH Zürich, Institute for Isotope Geology and Mineral Resources, 8092 Zürich, Switzerland*
[b] *Lamont-Doherty Earth Observatory, Palisades, New York, USA*
[c] *Department of Earth Sciences, University of Oxford, Oxford OX1 3PR, UK*

Received 23 September 2006; received in revised form 20 March 2007; accepted 29 March 2007

Editor: D. Rickard

Abstract

The extraction of a deepwater radiogenic isotope signal from marine sediments is a powerful, though under-exploited, tool for the characterisation of past climates and modes of ocean circulation. The radiogenic and radioactive isotope compositions (Nd, Pb, Th) of ambient deepwater are stored in authigenic Fe–Mn oxyhydroxide coatings in marine sediments, but the unambiguous separation of the isotopic signal in this phase from other sedimentary components is difficult and measures are needed to ensure its seawater origin. Here the extracted Fe–Mn oxyhydroxide phase is investigated geochemically and isotopically in order to constrain the potential and the limitations of the reconstruction of deepwater radiogenic isotope compositions from marine sediments.

Our results show that the isotope compositions of elements such as Sr and Os obtained from the Fe–Mn oxyhydroxide fraction are easily disturbed by detrital contributions originating from the extraction process, whereas the seawater isotope compositions of Nd, Pb and Th can be reliably extracted from marine sediments in the North Atlantic. The main reason is that the Nd, Pb and Th concentrations in the detrital phase of pelagic sediments are much lower than in the Fe–Mn oxyhydroxide fractions. This is reflected in Al/Nd, Al/Pb and Al/Th ratios of the Fe–Mn oxyhydroxide fractions, which are as low as or even lower than those of hydrogenetic ferromanganese crusts. Mass balance calculations illustrate that the use of the $^{87}Sr/^{86}Sr$ isotope composition to confirm the seawater origin of the extracted Nd, Pb and Th isotope signals is misleading. Even though the $^{87}Sr/^{86}Sr$ in the Fe–Mn oxyhydroxide fractions is often higher than the seawater Sr isotope composition, the corresponding detrital contribution does not translate into altered seawater Nd, Pb and Th isotope compositions due to mass balance constraints. Overall the rare earth element patterns, elemental ratios, as well as the mass balance calculations presented here highlight the potential of using authigenic Fe–Mn oxyhydroxide coatings as paleoceanographic archives for the analysis of past seawater Nd, Pb and Th isotope compositions.

Keywords: Neodymium; Lead; Thorium; Fe–Mn oxyhydroxides; Leaching; Mass balance

* Corresponding author. Now at: Bristol Isotope Group, Department of Earth Sciences, Wills Memorial Building, Queens Road, Bristol BS8 1RJ, UK. Tel.: +44 117 954 5235.
E-mail address: Marcus.Gutjahr@bristol.ac.uk (M. Gutjahr).
[1] Now at: IfM-GEOMAR, Leibniz Institute for Marine Sciences at the University of Kiel, 24148 Kiel, Germany.
[2] Now at: Department of Chemistry, University of Otago, PO Box 56, Union Place, Dunedin, New Zealand.

0009-2541/$ - see front matter © 2007 Elsevier B.V. All rights reserved.
doi:10.1016/j.chemgeo.2007.03.021

1. Introduction

The chemical extraction (leaching) of the seawater-derived Nd, Pb and Th isotope signal in the authigenic and early diagenetic Fe–Mn oxyhydroxide phase of marine sediments offers great potential for paleoceanographic and paleoclimatic purposes because it can yield essential information on sub-millennial fluctuations of marine environmental conditions. The benefit of using these seawater-derived radiogenic or radioactive trace metal isotope signatures is that they are not biased by biological processes, unlike other stable isotope or elemental ratio proxies. The analytical approach, however, is not trivial and an inherent caveat of the leaching of Fe–Mn oxyhydroxide coatings from marine sediments is the lack of unambiguous evidence for its unbiased deepwater origin.

Due to its residence time in seawater of 600 to 2000 years, Nd isotopes are increasingly used as a quasi-conservative water mass tracer for the present and past ocean (Frank, 2002; Goldstein and Hemming, 2003; Piotrowski et al., 2005). Lead is removed much faster from the water column, with an average residence time of only about 50 years in the Atlantic (Henderson and Maier-Reimer, 2002). Therefore, dissolved Pb isotope records are suitable archives for the detection of changes in local input sources (Frank, 2002; van de Flierdt et al., 2003; Foster and Vance, 2006). Dissolved Th isotopes in seawater are, as yet, a largely unemployed tool for the determination of changes in particle fluxes from the continents to the oceans because the $^{232}Th/^{230}Th$ is strongly controlled by the presence or absence of particulates in seawater (Guo et al., 1995; Robinson et al., 2004). As a consequence, higher particle fluxes from the continents to the open ocean should result in elevated seawater $^{232}Th/^{230}Th$. Considering the repeated deposition of ice rafted debris (IRD) layers during Heinrich events over the last glacial cycle, $^{232}Th/^{230}Th$ might serve as a good proxy for the correlation of North Atlantic sediment cores in the absence of conspicuous IRD layers.

Rare Earth Element (REE) porewater profiles of marine pelagic sediments suggest that under oxic to suboxic conditions trace metals (Sr, Nd, Os, Pb, Th) are scavenged from porewaters and incorporated into Fe–Mn oxyhydroxide coatings within the uppermost few centimetres below seafloor (Haley et al., 2004). These authors found most elevated REE concentrations in the upper 5 cm below seafloor, which indicates that most trace metals are incorporated into Fe–Mn oxyhydroxides within this zone or slightly below. Haley et al. (2004) also illustrated the effect of anoxic porewaters, where Fe–Mn oxyhydroxides are dissolved leading to trace metal concentrations in the pore waters, which are an order of magnitude higher than those found under oxic conditions (see also Elderfield and Sholkovitz, 1987; Thomson et al., 1993, 1995). Therefore, in studies employing the Fe–Mn oxyhydroxide fraction as paleoceanographic archives it is crucial to assess whether pore water anoxia prevailed at any time, which may have obliterated the original seawater signal.

It has also been suggested that, locally, the original authigenic Fe–Mn oxyhydroxide signal in marine sediments can be disturbed through pre-formed riverine Fe–Mn oxides on detrital material (Bayon et al., 2004). These authors concluded that the authigenic Fe–Mn oxyhydroxide signal in a sediment core from the Angola basin was biased through pre-formed detrital Fe oxide component associated with Congo river material transferred to the sedimentation site (Bayon et al., 2004). This issue is difficult to quantify in the interpretation of past seawater trace metal isotope compositions derived from Fe–Mn oxyhydroxide coatings. Core-top calibrations, directly comparing the extracted authigenic fraction with direct seawater measurements, are the best tool to date to detect such pre-formed oxides in the case of Nd and Th isotopes. For Pb isotopes, however, this test cannot be conducted because of anthropogenic disturbance of the natural seawater Pb isotope compositions (Schaule and Patterson, 1981; Alleman et al., 1999).

Measures are required to assess the reliability of the chemically extracted authigenic trace metal isotope signal. For this purpose, in previous studies using the Nd isotope composition of Fe–Mn oxyhydroxide coatings in pelagic sediments, the Sr isotope composition of the same fraction was measured to confirm the pure seawater origin of the Nd in the oxyhydroxide leachate (Rutberg et al., 2000; Piotrowski et al., 2004, 2005). Strontium is a conservative element in seawater with a residence time on the order of millions of years (Palmer and Elderfield, 1985; Henderson et al., 1994). The Sr isotope composition extracted from Fe–Mn oxyhydroxides in pelagic sediments of the past 100 kyr should thus reproduce the present-day seawater $^{87}Sr/^{86}Sr$ of 0.70918 (Henderson et al., 1994) if no significant Sr was leached from the detrital fraction. This test was successfully used in earlier studies carried out in the Southern Atlantic, where a seawater Sr isotope composition was indeed measured in the leachates. In contrast, the application of this monitor indicated significant detrital contributions to the leachates of Fe–Mn oxyhydroxides from several sites in the North Atlantic (Piotrowski, 2004). These offsets in Sr isotopes were not accompanied by obvious alterations of the Nd isotope compositions. Using core-top Nd isotope compositions measured in Fe–Mn oxyhydroxide leaches, in conjunction with the dissolved

SiO_2 concentration of the overlying water mass, Piotrowski (2004) observed very good agreement with direct seawater measurements with only two exceptions located near the African coast and on the Mid-Atlantic Ridge flank proximal to the Azores islands. Hence the good agreement in Nd isotope compositions between direct seawater measurements and leached core-top sediments presented by Piotrowski (2004) from the North Atlantic, despite non-hydrogenetic Sr isotope compositions measured in the same leachates, indicates that the Sr isotope composition as a sole guideline for the assessment of the seawater origin of the Nd isotope composition is probably too strict.

In this study we demonstrate why, regardless of the Sr or Os isotopic compositions, a reliable Nd isotopic composition of bottom seawater can be extracted from the Fe–Mn oxyhydroxide coatings of marine sediments in the North Atlantic, thus allowing the reconstruction of past water mass signatures. Secondly, it is shown that Pb, as well as Th isotope compositions in the same Fe–Mn oxyhydroxide fractions also reflect ambient seawater compositions. The complex paleoceanographic and paleoclimatic implications of the seawater Nd and Pb isotope evolution trends obtained from sediments along the Blake Ridge in the western North Atlantic are beyond the scope of this paper and will be discussed in separate publications.

2. Material and methods

Sediment cores along the Blake Ridge in the western North Atlantic have been recovered during R/V Knorr cruise 140 (KNR140). Samples used in this study were taken from core 51GGC (1790 m water depth; 32° N, 76° W) and 12JPC (4250 m water depth; 29° N, 73° W). In order to avoid blank contributions induced through sieving and successive rinsing of the sediments only bulk sediments were processed. Sediments were dried and ground for homogenisation. The method applied for the extraction of the seawater-derived Fe–Mn oxyhydroxide fraction was modified and combined from a variety of existing methods and is elucidated below (Chester and Hughes, 1967; Tessier et al., 1979; Ruttenberg, 1992; Rutberg et al., 2000; Bayon et al., 2002; Tovar-Sanchez et al., 2003; Piotrowski et al., 2004).

Samples were processed in acid-cleaned polypropylene 50 ml centrifuge tubes. Carbonate was removed using an Na acetate buffer in a shaker capped with Parafilm® to allow degassing of carbon dioxide during carbonate dissolution. The Na acetate buffer was employed because the usage of unbuffered 10% acetic acid (Bayon et al., 2002) was found to already significantly attack the Fe–Mn oxyhydroxide fraction. After centrifugation and decanting of the supernatant, loosely adsorbed metals were removed using a 1 M $MgCl_2$ solution (cf. Tessier et al., 1979). Following centrifugation and triple rinses in deionised water (Milli-Q system), the Fe–Mn oxyhydroxide coatings were dissolved by leaching the samples for 3 h in a shaker at room temperature in a 0.05 M hydroxylamine hydrochloride (HH)–15% distilled acetic acid–0.03 M Na–EDTA solution, buffered to pH 4 with analytical grade NaOH. Apart from elevating the pH of the leaching reagent, the NaOH is needed to avoid re-precipitation of the Na–EDTA. Alternatively, Na acetate can be used as a buffering reagent if NaOH clean enough for Sr isotope analyses (if required) should not be available.

In our study various leaching reagents for the dissolution of Fe–Mn oxyhydroxides have been tested.

Table 1
Summary of various reductive leaching reagents tested in the course of this study

Method	Reagent used	Comments
Boyle and Keigwin (1985)	1 M hydrazine–16% ammonia–0.25 M acetic acid 3 h in shaker at 65 °C	Too aggressive reagent. Irreproducible and spurious extracted Nd and Pb isotope compositions found. Hydrazine is carcinogen.
Test, this study	0.1 M oxalic acid 3 h in shaker at 65 °C	Too aggressive reagent. Irreproducible and spurious extracted Nd and Pb isotope compositions found.
Test, this study	1 M HH–15% acetic acid–0.1 M citric acid 3 h in shaker at 65 °C	Too aggressive reagent. Irreproducible and spurious extracted Nd and Pb isotope compositions found.
Chester and Hughes (1967); Bayon et al. (2002)	1 M HH–25% acetic acid 4 h in shaker at 95 °C	Too aggressive for sediments from the northwest Atlantic. Partly irreproducible and spurious extracted Nd and Pb isotope compositions found.
Chester and Hughes (1967); Rutberg et al. (2000); Piotrowski et al., (2004, 2005)	0.02 M HH–25% acetic acid 2–4 h in shaker at 20 °C	Works for Nd and Pb, but re-adsorption of authigenic Th during leaching.
Tovar-Sanchez et al. (2003)	Oxalate cocktail 3 h in shaker at 20 °C	Works, but tedious to prepare. High Sr blank.
Chester and Hughes (1967); Rutberg et al. (2000); Tovar-Sanchez et al. (2003); Piotrowski et al. (2004)	0.05 M HH–15% acetic acid–0.03 M Na–EDTA 2–3 h in shaker at 20 °C	Best possible reagent found for the gentle extraction of all trace metals.

Chester and Hughes (1967) conducted leaching experiments with ferromanganese crust powders using (a) diluted acetic acid, (b) diluted hydroxylamine hydrochloride, or (c) a mixture of the two reagents. One of their findings was that the stand-alone usage of acetic acid preferentially dissolves Fe oxides, whereas very dilute (0.02 M) already effectively dissolves Mn oxides with only minor dissolution of Fe oxides. The combined usage of 25% acetic acid with 0.02 M HH at room temperature for 4 h in a shaker effectively dissolved most of the Fe and the Mn oxides. Most subsequent leaching protocols referred to this pioneer work. In Table 1 a variety of different leaching reagents are presented, which have been tested in the course of this study. Further alternative chemical extraction methods can be found in Bayon et al. (2002). A summary chart displaying our recommended individual leaching steps for the extraction of the Fe–Mn oxyhydroxide fraction is shown in Fig. 1.

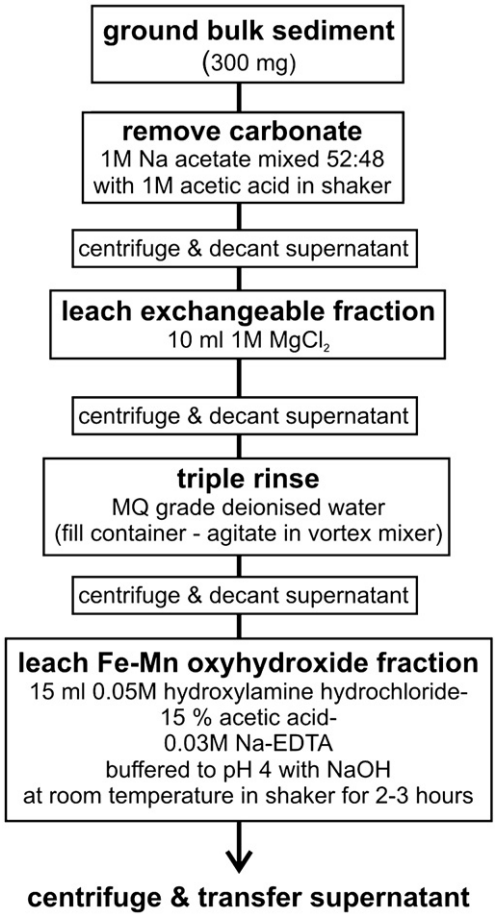

Fig. 1. Recommended analytical procedure for the extraction of the Fe–Mn oxyhydroxide coatings.

In addition, the detrital fraction was extracted from the sediments to obtain the complimentary detrital isotope signal for each of the Fe–Mn oxyhydroxide fractions. Because the leaching protocol described above does not extract the Fe–Mn oxyhydroxide fraction quantitatively, a second leach with the above HH–acetic acid–Na–EDTA leach was applied for 24 h to guarantee complete removal of residual Fe–Mn oxyhydroxide coatings. A further two rinses with deionised water were applied prior to treatment of the samples with *aqua regia* to destroy organic matter. The remaining detrital sediment fraction was dissolved by pressure digestion in a concentrated $HF–HNO_3$ mixture.

On a set of nine sediment samples a small fraction of the first (3 h) and the second (24 h) Fe–Mn oxyhydroxide leachate, as well as an aliquot of the detrital fraction was separated for the determination of major and trace element concentrations, measured by ICP-OES and ICP-MS at the Geological Institute of the University of Kiel (Germany). Results of the major, selected trace and rare earth element analyses are shown in Table 2. The individual Sr, Nd, Os, Pb and Th isotope results are displayed in Table 3.

The first Fe–Mn oxyhydroxide leach and the detrital fraction were split into separate aliquots for the extraction of Sr, Nd and Pb. For a subset of nine Fe–Mn oxyhydroxide coating samples, additional aliquots were taken for Th isotope measurements of the Fe–Mn oxyhydroxide fraction, as well as a subset of seven samples for Os isotope analyses.

Separation and purification of the individual elements followed standard procedures, for Sr (Horwitz et al., 1992), Nd (Cohen et al., 1988), Os (Birck et al., 1997; Klemm et al., 2005), Pb (Lugmair and Galer, 1992) and Th (Luo et al., 1997). All total procedural blanks, comprising reagent and lab procedural blanks, were analysed by ICP-MS at the University of Kiel. The Sr procedural blank for the Fe–Mn oxyhydroxide fraction were high due to the use of analytical grade NaOH for buffering of the leach solution, averaging 22.2 ng and contributing between 0.4 and 8.7% of the Sr Fe–Mn oxyhydroxide coating signal. The Sr isotope ratios in the mass balance calculation were corrected for this blank contribution, which was found to have no significant effect on our conclusions. Corrected $^{87}Sr/^{86}Sr$ isotope ratios changed on the third or fourth decimal place (at most 0.0005 for sample 12JPC-55 cm), whereas small contributions from the detrital fraction to the leached fraction had much more severe effects on the Sr isotope composition (as much as 0.0128 for 12JPC-20 cm, Table 2). The total Sr procedural blank for the detrital fraction was 1.7 ng and is less than 0.004% of

Table 2
Selected major and trace element concentrations

	Al_2O_3	Fe_2O_3	MnO	CaO	TiO_2	Sr	Pb	Th	U	La	Ce	Pr	Nd	Sm	Eu	Gd	Tb	Dy	Ho	Er	Tm	Yb	Lu
	μg/g	μg/g	μg/g	μg/g	μg/g	ng/g	ng/g	ng/g	ng/g	ng/g	ng/g	ng/g	ng/g	ng/g	ng/g	ng/g	ng/g	ng/g	ng/g	ng/g	ng/g	ng/g	ng/g
First Fe–Mn oxyhydroxide leach fraction (3 h)																							
51GGC																							
60 cm	137	240	7.9	1261	2.3	14059	1366	1106	87	3594	5904	945	3515	736	165	714	111	646	126	318	47	294	42
270 cm	185	406	9.4	363	2.9	2451	2183	1941	86	4412	9013	1289	4946	1066	236	1019	157	891	171	423	62	382	54
316 cm	93	411	3.8	423	2.3	1083	1140	1042	80	2335	4069	660	2495	530	114	508	75	413	78	190	27	167	23
350 cm	190	718	6.5	511	4.0	2181	2630	1483	52	3414	7540	1010	3895	876	187	837	124	676	125	302	44	273	38
390 cm	45	273	4.9	1044	2.2	3498	1096	860	164	2014	3572	582	2312	520	117	531	77	435	84	206	29	177	26
400 cm	117	333	2.0	195	2.8	1130	1786	1446	105	1984	4246	660	2642	658	146	654	94	506	92	218	30	186	26
12JPC																							
55 cm	369	1348	1864	226	34.4	1368	6346	2657	44	3446	15486	1118	4189	927	187	844	126	669	120	285	41	247	34
85 cm	311	920	371	249	14.1	1121	6120	2551	42	3405	11577	1182	4684	1126	233	1040	151	780	136	311	43	260	36
263 cm	291	731	6.3	222	4.6	870	4317	2576	47	2710	8234	1042	4248	1060	224	954	136	679	114	254	35	209	28
Second Fe–Mn oxyhydroxide leach fraction (24 h)																							
51GGC																							
60 cm	323	615	7.2	401	4.8	3800	736	625	61	1424	2979	413	1561	328	71	297	44	237	42	96	13	74	10
270 cm	390	984	7.6	114	7.1	1408	1530	1104	68	2500	6161	764	2898	588	123	514	76	411	76	183	26	157	21
316 cm	180	754	4.2	102	4.4	458	974	327	34	720	1587	213	805	165	33	147	21	111	20	45	6	35	5
350 cm	329	1187	9.5	236	6.0	1036	2156	934	39	1756	4303	542	2118	476	95	429	62	320	57	134	19	115	16
390 cm	200	606	5.4	376	6.0	817	394	234	61	544	1097	157	611	139	29	130	18	90	16	37	5	31	4
400 cm	304	653	5.7	74	8.2	454	435	286	38	657	1497	198	753	165	31	145	19	90	16	36	5	30	4
12JPC																							
55 cm	440	1639	215	108	19.9	864	2087	1235	31	1765	6201	506	1826	362	67	306	44	228	40	95	13	80	11
85 cm	461	1763	68	142	16.6	880	2780	1504	32	2223	6509	652	2415	499	94	426	61	303	52	119	17	98	13
263 cm	550	1602	19	187	10.9	986	2208	1655	39	2339	6524	720	2705	568	108	478	67	326	54	122	17	98	13
Detrital fraction																							
51GGC																							
60 cm	28,871	12,589	88	1022	1746	54,459	6412	6170	2048	24,399	42,820	5112	17,300	2814	510	2244	302	1857	346	970	129	1043	132
270 cm	41,772	19,633	105	1371	2641	85,251	11,890	10,703	3380	36,607	65,166	7871	26,630	4414	822	3595	510	3153	608	1699	243	1861	251
316 cm	24,216	11,031	83	1442	1543	31,924	2701	1867	657	7562	14,664	1710	5973	1044	202	875	128	816	159	453	66	513	70
350 cm	42,985	24,317	156	2130	2981	97,652	9403	9429	2668	32,739	63,228	8065	27,354	4614	875	3781	551	3394	667	1848	271	2007	276
390 cm	25,795	11,961	96	2411	2071	82,316	6047	5204	1678	17,698	35497	4296	15,338	2760	478	2319	325	2091	395	1143	154	1301	168
400 cm	38,506	16,451	138	2284	2906	97,746	8045	7923	2415	30,282	58,156	6904	24,104	4115	740	3376	481	3126	610	1759	248	2008	265
12JPC																							
55 cm	55,311	26,941	214	3756	3054	134,832	10,005	8208	1997	35,010	63,651	7325	24,830	4009	781	3183	430	2826	529	1542	194	1699	201
85 cm	48,958	34,294	263	2139	3663	154,726	12,788	13,577	2882	55,414	102,186	12,050	40,821	6558	1258	5203	742	4570	888	2483	358	2704	361
263 cm	50,519	38,049	298	1821	4082	145,795	15,413	14784	3919	37,681	81,959	11,161	39,466	7365	1434	5980	906	5624	1116	3080	462	3377	471

All concentrations in the table are normalised to gram of leached bulk sediment (μg/g for major elements, ng/g for trace elements).
Note that the second leach, applied for 24 h in a shaker, was not able to extract more material than the first leach, which was only applied for 3 h.

Table 3
Sr, Nd, Os, Pb and Th isotope ratios of the coating and detrital fractions analysed in the course of this study

Core	Depth in core (cm)		$^{87}Sr/^{86}Sr$ ±0.00049[a]	$^{143}Nd/^{144}Nd$ ±0.000014	ε_{Nd} ±0.27	$^{187}Os/^{188}Os$ ±0.0006	Os [pg/g]	$^{206}Pb/^{204}Pb$ ±0.0016	$^{207}Pb/^{204}Pb$ ±0.0017	$^{208}Pb/^{204}Pb$ ±0.0052	$^{208}Pb/^{206}Pb$ ±0.00015	$^{207}Pb/^{206}Pb$ ±0.00003	$^{232}Th/^{230}Th$
51GGC	60	Coating	0.70918	0.512127	−10.0	1.053±0.005	9.53	19.1337	15.6906	39.1620	2.04678	0.82007	n.d.
51GGC	270	Coating	0.70958	0.512114	−10.2	n.d.	n.d.	19.2187	15.6844	39.2735	2.04346	0.81610	n.d.
51GGC	316	Coating	0.70949	0.512109	−10.3	1.269±0.014	2.55	19.1229	15.6781	39.1306	2.04630	0.81987	n.d.
51GGC	350	Coating	0.70977	0.512088	−10.7	1.154±0.009	7.02	19.0723	15.6672	39.0757	2.04881	0.82147	n.d.
51GGC	390	Coating	0.70894	0.512164	−9.3	n.d.	n.d.	19.0280	15.6730	38.9298	2.04593	0.82367	n.d.
51GGC	400	Coating	0.70983	0.512154	−9.4	1.177±0.006	2.09	18.9804	15.6622	38.8977	2.04942	0.82520	n.d.
12JPC	55	Coating	0.71500	0.511963	−13.2	1.081±0.015	1.22	19.3772	15.6928	39.5909	2.04318	0.80986	n.d.
12JPC	85	Coating	0.71391	0.512069	−11.1	1.157±0.008	1.69	19.1117	15.6650	39.1725	2.04968	0.81966	n.d.
12JPC	263	Coating	0.71239	0.512119	−10.1	1.095±0.014	1.68	18.9438	15.6543	38.9209	2.05454	0.82636	n.d.
51GGC	60	Detrital	0.72076	0.512076	−11.0	n.d.	n.d.	18.9916	15.6499	38.8863	2.04755	0.82404	n.d.
51GGC	270	Detrital	0.72228	0.512083	−10.8	n.d.	n.d.	19.0187	15.6492	38.9023	2.04548	0.82283	n.d.
51GGC	316	Detrital	0.72108	0.512057	−11.3	n.d.	n.d.	18.8819	15.6247	38.7390	2.05165	0.82750	n.d.
51GGC	350	Detrital	0.72659	0.512003	−12.4	n.d.	n.d.	18.9437	15.6252	38.8736	2.05206	0.82482	n.d.
51GGC	390	Detrital	0.71789	0.512071	−11.1	n.d.	n.d.	18.9218	15.6196	38.7637	2.04863	0.82548	n.d.
51GGC	400	Detrital	0.72307	0.512033	−11.8	n.d.	n.d.	19.1015	15.6363	38.9689	2.04010	0.81859	n.d.
12JPC	55	Detrital	0.72861	0.511868	−15.0	n.d.	n.d.	18.3156	15.5268	38.5224	2.10325	0.84774	n.d.
12JPC	85	Detrital	0.73057	0.511943	−13.6	n.d.	n.d.	18.6927	15.5893	38.8042	2.07590	0.83398	n.d.
12JPC	263	Detrital	0.73207	0.512012	−12.2	n.d.	n.d.	18.8683	15.6246	38.9345	2.06349	0.82809	n.d.
51GGC	40	Coating	0.71152	0.512117	−10.2	n.d.	n.d.	19.0866	15.6862	39.1302	2.05015	0.82184	43,460±70
51GGC	160	Coating	0.71046	0.512140	−9.7	n.d.	n.d.	19.1674	15.6912	39.1748	2.04387	0.81865	40,100±80
51GGC	300	Coating	0.71287	0.512107	−10.4	n.d.	n.d.	19.2333	15.6864	39.2660	2.04152	0.81557	47,500±140
51GGC	330	Coating	0.71155	0.512091	−10.7	n.d.	n.d.	19.0970	15.6686	39.1061	2.04784	0.82048	58,890±220
51GGC	370	Coating	0.71497	0.512106	−10.4	n.d.	n.d.	19.0683	15.6648	39.0736	2.04917	0.82152	70,090±230
51GGC	371	Coating	0.71356	0.512085	−10.8	n.d.	n.d.	19.0678	15.6659	39.0737	2.04919	0.82158	75,530±210
51GGC	405	Coating	0.71674	0.512132	−9.9	n.d.	n.d.	18.9927	15.6664	38.9289	2.04968	0.82487	63,490±180
12JPC	20	Coating	0.72199	0.511992	−12.6	n.d.	n.d.	19.2170	15.6811	39.4023	2.05038	0.81600	24,130±40
12JPC	233	Coating	0.72176	0.512126	−10.0	n.d.	n.d.	18.9306	15.6485	38.8740	2.05349	0.82662	73,240±160

Summary of all isotope results obtained in the course of this study. Sr isotope results for the upper nine Fe–Mn oxyhydroxide coating samples have been corrected for a blank contribution, as have the Os samples. The lowermost nine Sr isotope results, however, are not corrected for the blank contribution because these samples were not analysed by ICP-MS and hence trace element concentration data are not available.

[a] The cited $^{87}Sr/^{86}Sr$ uncertainty also includes the inaccuracy induced by blank contributions to the Fe–Mn oxyhydroxide fractions. The long-term $^{87}Sr/^{86}Sr$ reproducibility without this blank contribution is ±0.000025, which applies to the detrital samples. Os isotopes have been measured with N-TIMS, the remaining isotope systems by MC-ICPMS on a Nu Plasma instrument. Also shown are Os concentrations for the Fe–Mn oxyhydroxide fractions analysed isotopically in this study.

the detrital Sr concentration. Procedural blanks for Nd were <30 pg for the oxyhydroxide fraction and <315 pg for the detrital fraction, with all blanks being smaller than 0.1% of the total amount of Nd present in each sample. The total procedural blank for Os was below 0.7 pg and the applied blank correction was between 5 and 20%. For Pb the procedural blank in the Fe–Mn oxyhydroxide fraction was 1.03 ng and always below 0.35% of the total Pb concentration. In the detrital Pb fraction, the procedural blank was 1.31 ng and below 0.33% of the total amount of Pb present in the samples. Total procedural blanks for ^{232}Th were <10 pg and were negligible. Procedural blanks for ^{230}Th were below the detection limit of the secondary electron multipliers (SEMs) on the Nu Plasma MC-ICPMS.

Measurements of the Sr, Nd, Pb and Th isotopes were carried out on a Nu Plasma MC-ICPMS at ETH Zürich using the exponential law to correct for instrumental mass fractionation (Rehkamper et al., 2001). The long-term analytical reproducibility quoted in this section and in Table 3 refers to the machine reproducibility for the various standard solutions, with exception of the respective uncertainty for the Sr isotope ratios. Interfering ^{86}Kr (from the Ar carrier gas) and possible ^{87}Rb contributions on the respective Sr masses have been monitored through the simultaneous measurement of ^{83}Kr and ^{85}Rb. Interference-corrected ^{87}Sr/^{86}Sr was adjusted for mass bias by normalising to ^{86}Sr/^{88}Sr of 0.1194 (Nier, 1938; Steiger and Jager, 1977). Linearly interpolated zero beam intensities on 1/3 masses above and below the mass of interest have been subtracted from the respective ion beams. All reported Sr isotope results were normalised to ^{87}Sr/^{86}Sr=0.710245 for the NIST SRM987 Sr standard. The long-term reproducibility for repeated measurements of the NIST SRM987 Sr standard was 0.000025 (2σ; n=70). The ^{87}Sr/^{86}Sr uncertainty quoted in Table 3 (±0.00049) also includes the maximum offset induced by the blank contribution and therefore only applies to the Fe–Mn oxyhydroxide coating samples.

Measured ^{143}Nd/^{144}Nd was corrected for the instrumental mass bias applying a ^{146}Nd/^{144}Nd of 0.7219. All reported Nd isotope results were normalised to a ^{143}Nd/^{144}Nd of 0.512115 for the JNdi-1 standard (Tanaka et al., 2000). The long-term reproducibility for repeated measurements of the JNdi-1 standard was ±0.27 ε_{Nd} (2σ; n=70). The ^{143}Nd/^{144}Nd results presented here are expressed in standard epsilon notation relative to a Chondrite Uniform Reservoir (CHUR):

$$\varepsilon_{Nd} = \left[\frac{^{143}Nd/^{144}Nd_{sample}}{^{143}Nd/^{144}Nd_{CHUR}} - 1 \right] \times 10^4$$

(^{143}Nd/^{144}Nd$_{CHUR}$=0.512638 (Jacobsen and Wasserburg, 1980)).

Lead isotopes were measured using a Tl-doping procedure (Walder and Furuta, 1993; Belshaw et al., 1998) with a Pb/Tl ~4. The expected offset to TIMS Pb isotope data (cf., Thirlwall, 2002) are accounted for by normalising all respective Pb isotope compositions to the triple spike TIMS Pb ratios for NIST SRM 981 reported by Galer and Abouchami (1998).

Thorium isotope compositions (^{232}Th/^{230}Th) in the Fe–Mn oxyhydroxide fractions were measured using an external normalisation technique by doping with the CRM 145 U metal standard solution (formerly NIST SRM 960). The instrumental mass bias was corrected for by normalising to a ^{238}U/^{235}U value of 137.88 (Steiger and Jager, 1977). Individual measurements were split into two cycles due to the cup configuration of the MC-ICPMS (Table 4). Using this setup, the minor ^{230}Th ion beam was monitored on SEM 2 (IC2), simultaneously with ^{235}U and ^{238}U on Faraday detectors in the first cycle, while ^{238}U, ^{235}U and ^{232}Th were monitored subsequently on Faraday collectors during a second analysis sequence (Table 4). The relative gain between the Faraday collectors and each SEM was calibrated against the CRM 145 U standard solution doped with a ^{233}U/^{229}Th spike. All isotope ratios were corrected for the minor amounts of natural ^{238}U, ^{235}U, ^{234}U, ^{232}Th and ^{230}Th present in the artificial spike. After a preceding peak tailing characterisation of the major ^{232}Th ion beam monitoring the mass range between 230.6 and 228.5 on

Table 4
Collector array of the Nu Plasma MC-ICPMS used for the Th isotope analysis at the ETH, Zürich

	F (+2)	F (+1)	F (Ax)	F (−1)	F (−2)	IC0 (−3)	F (−4)	IC1 (−5)	F (−6)	IC2 (−7)
Zero 1	238.5	237.5		235.5	234.5	233.5	232.5			229.5
Zero 2	239.5	238.5		236.5	235.5	234.5	233.5			230.5
Cycle 1		^{238}U			^{235}U	^{234}U				^{230}Th
Cycle 2	^{238}U			^{235}U			^{232}Th			

Due to the cup configuration the measurements have been split into two cycles, allowing the determination of the ^{230}Th abundance in cycle one and the ^{232}Th abundance in cycle two. Numbers in brackets refer to mass differences (amu) to the axial Faraday collector.

the SEM, the linearly interpolated half mass zeros on ^{230}Th have been corrected by −8.84%. The Th104 standard supplied by C. Innocent reproduced at 27,260± 89 (n=41, 2σ) and the Th105 standard at 217,080±1428 (n=22, 2σ). Abundance sensitivity is on the order of 2.5 to 5 ppm amu^{-1}(cf., Andersen et al., 2004). Thorium isotope ratios have been age-corrected for the decay of ^{230}Th since time of incorporation into the Fe–Mn oxyhydroxide coatings (i.e., depositional age of the sediment).

Osmium isotope compositions and the total amount of Os within each sample as determined by isotope dilution, were obtained by negative thermal ionisation mass spectrometry (N-TIMS) following published methods (Creaser et al., 1991; Volkening et al., 1991; Birck et al., 1997). The external reproducibility of the Os isotope measurements over the course of 3 years, determined through repeated measurements of an internal Os-standard was ^{187}Os/^{188}Os=0.1081±0.0006 (2σ) (n=18).

Calendar ages used in Fig. 2A are based on conventional ^{14}C ages published earlier by Keigwin (2004); transformed into calendar years using the marine radiocarbon age calibration Marine04 of Hughen et al. (2004) assuming ΔR=0.

3. Results

3.1. Strontium isotopes

Many of the leached Fe–Mn oxyhydroxide fractions shown in Table 3 yielded ^{87}Sr/^{86}Sr that are offset from the expected seawater value of 0.70918 (Henderson et al., 1994). Generally ^{87}Sr/^{86}Sr offsets were higher in the deeper core than in the shallow core. The most radiogenic Sr was found in the deep core (^{87}Sr/^{86}Sr= 0.72199 for JPC12 — 20 cm). Hence for the vast majority of the Fe–Mn oxyhydroxide leachates the ^{87}Sr/^{86}Sr suggests a significant detrital Sr contribution to the leached fraction (Table 3). The Fe–Mn oxyhydroxide fractions contained between 0.87 and 2.45 µg Sr per gram of leached sediment (Tables 2 and 6). Only coating sample 51GGC — 60 cm contained relatively high Sr concentrations in the Fe–Mn oxyhydroxide fraction, which is possibly be due to incomplete removal of the carbonate fraction during the decarbonation step (14.06 µg/g of leached Sr in Fe–Mn oxyhydroxide fraction). Compared with the sum of total Sr present in both the Fe–Mn oxyhydroxide-and detrital fractions, only about 0.5 to 3.9% of the total Sr in the sediments is seawater-derived (with the exception of 51GGC — 60 cm, in which 19.4% of total Sr in the oxyhydroxide fraction originated from seawater).

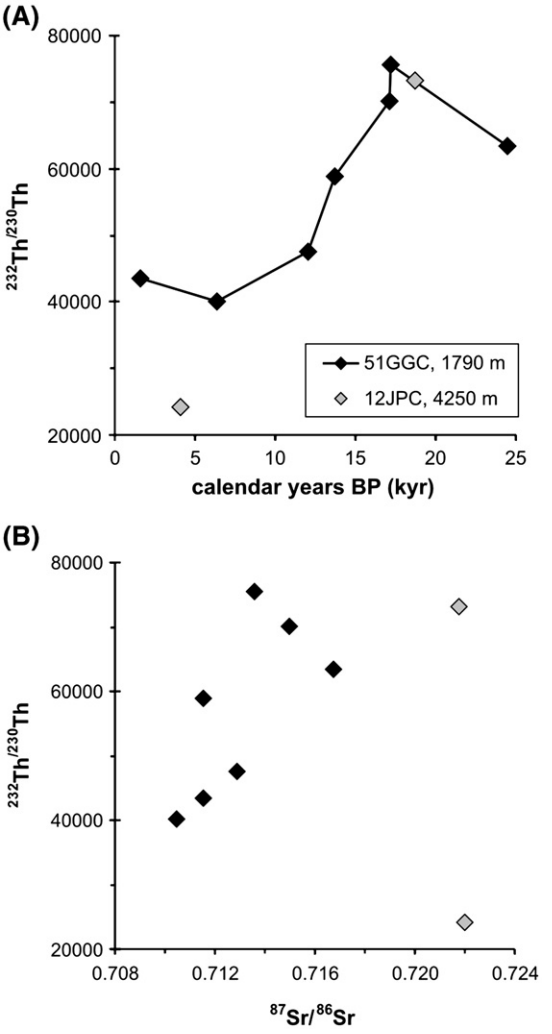

Fig. 2. (A) Th isotope time series for core 51GGC in 1790 m, and two additional results from core 12 JPC in 4250 m. The cores show the same decrease in Th isotope composition during the transition from the early deglaciation to the Holocene. (B) Th and Sr isotope cross-plot. 2σ error bars are smaller than symbol size.

3.2. Thorium isotopes

In the shallow core 51GGC the ^{232}Th/^{230}Th in the leached Fe–Mn oxyhydroxide fractions ranges from 40,100 in Holocene samples to 75,530 at the end of the Last Glacial Maximum (17.2 ka BP; Fig. 2A and Table 3). Deep core 12JPC is consistent with the trend indicated by the shallow core for two measured samples. The Holocene sample at 20 cm depth yielded a ^{232}Th/^{230}Th of 24,130 and one sample representing the deglaciation gave 73,240. The ^{232}Th/^{230}Th ratios presented here are in the range of present-day ^{232}Th/^{230}Th values published from nearby locations close to Cape Hatteras

north of Blake Ridge, which range from $^{232}Th/^{230}Th$ of 122,840 in surface waters to $^{232}Th/^{230}Th$ of 27,990 at 750 m water depth (Guo et al., 1995). Seawater $^{232}Th/^{230}Th$ compositions for the LGM and the deglaciation are not available for comparison.

3.3. Osmium isotopes

Only one out of seven Fe–Mn oxyhydroxide fractions yielded the present-day seawater $^{187}Os/^{188}Os$ of ~1.06 (Levasseur et al., 1998; Peucker-Ehrenbrink and Ravizza, 2000). In Fig. 3 the $^{187}Os/^{188}Os$ of core 51GGC shows a shift towards more radiogenic continental $^{187}Os/^{188}Os$ accompanied by only minor offsets from seawater $^{87}Sr/^{86}Sr$. Results from deep core 12JPC indicate less detrital contribution to the authigenic $^{187}Os/^{188}Os$, which, however, correspond to significant offsets in $^{87}Sr/^{86}Sr$. The large offset from seawater $^{187}Os/^{188}Os$ is explicable by the low Os concentrations in the respective aliquots, ranging from 1.22 to 9.53 pg per gram of leached bulk sediment (Table 3). The very low abundance of Os in the oxyhydroxide fraction reflects its very low seawater concentrations, and is responsible for the high susceptibility of the leached isotope ratios to detrital contamination.

3.4. Rare earth elements

Fig. 4 shows the results for rare earth element (REE) analyses carried out on leachates of a set of 9 samples from the two core locations. The PAAS-normalised REE plot of the two Fe–Mn oxyhydroxide fractions shows a distinct mid REE (MREE) enrichment (Fig. 4A, B), which is not evident in the detrital fraction (Fig. 4C). This MREE enrichment is essentially identical to marine pore water REE patterns where particulate Fe^{3+} oxides are reduced and dissolved, thereby releasing scavenged REE (Haley et al., 2004). In contrast and according to expectations, the detrital phases of the same sediment samples display flat PAAS-normalised REE patterns (Fig. 4C).

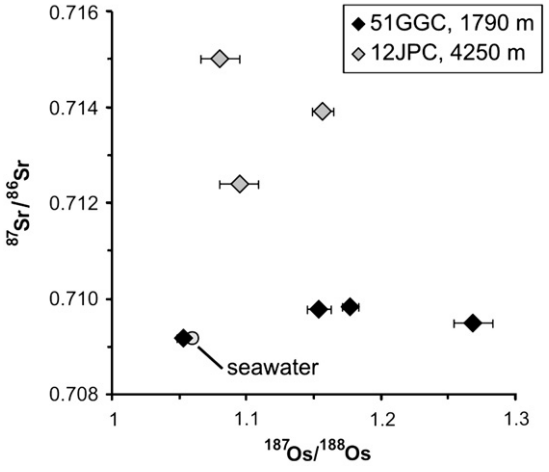

Fig. 3. Sr and Os isotope cross-plot, demonstrating the offset for the majority of samples from seawater compositions. Only one sample corresponds to present day seawater.

3.5. Elemental ratios

Another independent tool to evaluate the characteristics of an extracted phase from marine sediments is its aluminium content. Compared with crustal rocks or detrital sediments, hydrogenetic ferromanganese crusts generally display low Al/Nd and Al/Pb due to the preferential incorporation of trace metals over Al (see Hein et al. (1999) for a compilation). For comparison we chose data obtained from ferromanganese crusts from the Central Equatorial and the Southern Pacific, which are a good approximation for a hydrogenetic Fe–Mn oxyhydroxide end member, as these locations are most remote from any continental source area, representing the most pristine hydrogenetic geochemical composition. In Table 5, Al, Nd, Pb and Th concentrations as well as elemental ratios are shown for selected abyssal ferromanganese crusts (data from Hein et al., 1999), and the different sediment fractions analysed in this study are displayed for comparison. The Al/Nd, Al/Pb and Al/Th for the Blake Ridge sediment fractions are plotted in Fig. 5 (note the log scale of the *y*-axis). For the first (3 h-leached) Fe–Mn oxyhydroxide fraction, Al/Nd values are even lower than those for ferromanganese crusts in Table 5, averaging 13.2. The second (24 h-leached) Fe–Mn oxyhydroxide leaches yielded Al/Nd in the range of the Fe–Mn crusts (average Al/Nd=61). The ratios in the detrital fraction of the sediment samples are entirely different from those in the first Fe–Mn oxyhydroxide fraction (average Al/Nd=495; Table 5, Fig. 5).

For Al/Pb, the first leaches have comparable elemental ratios to Pacific abyssal ferromanganese crusts, Al/Pb averaging 18.3 and 11, respectively (Table 5). The second Fe–Mn oxyhydroxide leach fraction has somewhat elevated ratios (Al/Pb=83), whereas Al/Pb of the remaining detrital fractions are an order of magnitude higher, with an average of 1271 (see also Fig. 5).

The ratio of Al over Th (^{232}Th), in contrast, reflects the very high particle reactivity of Th compared with Nd or Pb. Ferromanganese crust data displayed in Table 5 have a relatively high Al/Th but this is due to low

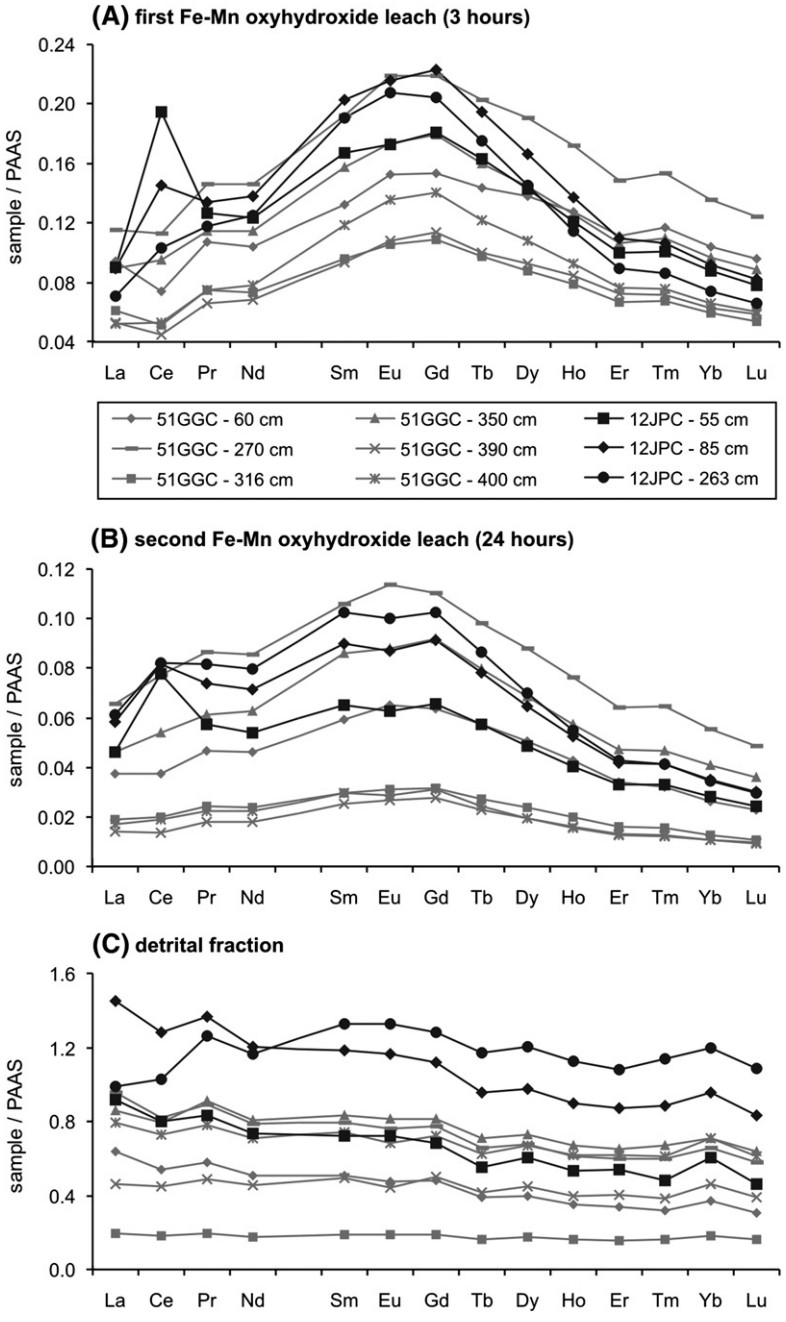

Fig. 4. Post-Archean Australian average shale normalised (PAAS) REE multi-element plots for two sequential Fe–Mn oxyhydroxide leaching phases and the respective detrital fraction. The second leach was applied to ensure complete removal of the Fe–Mn oxyhydroxide phase. PAAS data are from McLennan (1989).

concentrations of dissolved or particulate ^{232}Th in the deep Pacific (Table 5) (Swarzenski et al., 2003). The continental slope and rise of the eastern North America is an area of high turbidity and high particle fluxes from the continent to the deep Atlantic (Eittreim et al., 1969; Eittreim et al., 1976; McCave, 1986; Biscaye et al., 1988). The waters along this continental margin have highly elevated dissolved ^{232}Th concentrations due to particle–seawater interaction, reflected in very low Al/Th recorded in Fe–Mn oxyhydroxide coatings (Guo

Table 5
Al, Nd, Pb and Th concentrations of ferromanganese crusts and sediment fractions

	Al (mg/g)[a,b]	Nd (ppm)	Pb (ppm)	Th (ppm)	Al/Nd	Al/Pb	Al/Th
Central Equatorial Pacific[a]							
Marshall Is.	11.9	170	1799	10.2	70	7	1167
NW of Marshall Is.	12.0	238	1689	–	50	7	–
Johnston I.	14.2	210	1871	17.7	68	8	802
South Pacific[a]	15.8	226	741	2.1	70	21	7535
Atlantic[a]	31.6	–	1133	54.2	–	28	583
				Average:	65	11	3168
This study	Al (μg/g)[c]	Nd (μg/g)[c]	Pb (μg/g)[c]	Th (μg/g)[c]	Al/Nd	Al/Pb	Al/Th
First Fe–Mn oxyhydroxide leach (3 h)							
51GGC — 60 cm	36.1	3.52	1.37	1.11	10.3	26.4	32.7
51GGC — 270 cm	49.0	4.95	2.18	1.94	9.9	22.5	25.3
51GGC — 316 cm	24.7	2.50	1.14	1.04	9.9	21.7	23.7
51GGC — 350 cm	50.4	3.89	2.63	1.48	12.9	19.2	34.0
51GGC — 390 cm	11.9	2.31	1.10	0.86	5.2	10.9	13.9
51GGC — 400 cm	31.0	2.64	1.79	1.45	11.7	17.4	21.5
12JPC — 55 cm	97.7	4.19	6.35	2.66	23.3	15.4	36.8
12JPC — 85 cm	82.2	4.68	6.12	2.55	17.6	13.4	32.2
12JPC — 263 cm	77.0	4.25	4.32	2.58	18.1	17.8	29.9
				Average:	13.2	18.3	28
Second Fe–Mn oxyhydroxide leach (24 h)							
51GGC — 60 cm	85	1.56	0.74	0.63	55	116	137
51GGC — 270 cm	103	2.90	1.53	1.10	36	67	93
51GGC — 316 cm	48	0.81	0.97	0.33	59	49	145
51GGC — 350 cm	87	2.12	2.16	0.93	41	40	93
51GGC — 390 cm	53	0.61	0.39	0.23	87	134	226
51GGC — 400 cm	80	0.75	0.43	0.29	107	185	281
12JPC — 55 cm	116	1.83	2.09	1.24	64	56	94
12JPC — 85 cm	122	2.41	2.78	1.50	51	44	81
12JPC — 263 cm	146	2.70	2.21	1.66	54	66	88
				Average:	61	84	138
Detrital fraction							
51GGC — 60 cm	7640	17.30	6.41	6.17	442	1192	1238
51GGC — 270 cm	11054	26.63	11.89	10.70	415	930	1033
51GGC — 316 cm	6408	5.97	2.70	1.87	1073	2372	3433
51GGC — 350 cm	11375	27.35	9.40	9.43	416	1210	1206
51GGC — 390 cm	6826	15.34	6.05	5.20	445	1129	1312
51GGC — 400 cm	10190	24.10	8.04	7.92	423	1267	1286
12JPC — 55 cm	14637	24.83	10.00	8.21	589	1463	1783
12JPC — 85 cm	12956	40.82	12.79	13.58	317	1013	954
12JPC — 263 cm	13369	39.47	15.41	14.78	339	867	904
				Average:	495	1271	1461

Selection of Al, Nd, Pb and Th concentrations for Pacific ferromanganese crusts, as compiled in Hein et al. (1999), and the respective elemental ratios. For comparison, the concentrations and elemental ratios for samples analysed during this study are displayed. Concentrations for the different fractions are given in μg per gram of bulk sediment used. Elemental ratios are displayed in Fig. 5.

[a] Literature data from Hein et al. (1999).

[b] Where possible Al concentrations were calculated on a loss-on-ignition free base.

[c] Concentration data given for sediments analysed in this study are normalised to μg per gram of raw sediment weighed in.

et al., 1995). More importantly for our purposes, however, the two sequential leaching phases, as well as the detrital fraction in the sediments show similar systematic differences analogous to Al/Nd and Al/Pb, which are independent of the age of the sediment. Therefore the very low Al/Nd, Al/Pb and Al/Th in the first Fe–Mn oxyhydroxide leach fraction support the hydrogenetic origin of all three extracted trace metals.

4. Discussion

4.1. REE patterns

The REE patterns shown in Fig. 4, obtained from Fe–Mn oxyhydroxide fractions through reductive leaching of oxic sediments, are similar to anoxic marine pore water REE patterns (Haley et al., 2004). These authors attributed the MREE enrichment to the release of REE from Fe oxide phases under reducing conditions, which preferentially release the incorporated MREE. Conversely, Hannigan and Sholkovitz (2001) reported MREE enrichments in waters from a variety of rivers being tightly coupled with dissolved phosphate concentrations. Hence the MREE enrichment could be caused by two different phases, either by leaching of phosphates or by release of REE from the Fe–Mn oxyhydroxides. Ohr et al. (1994) argued that the REE budget obtained during leaching of argillaceous sediments may be controlled by dissolution of authigenic

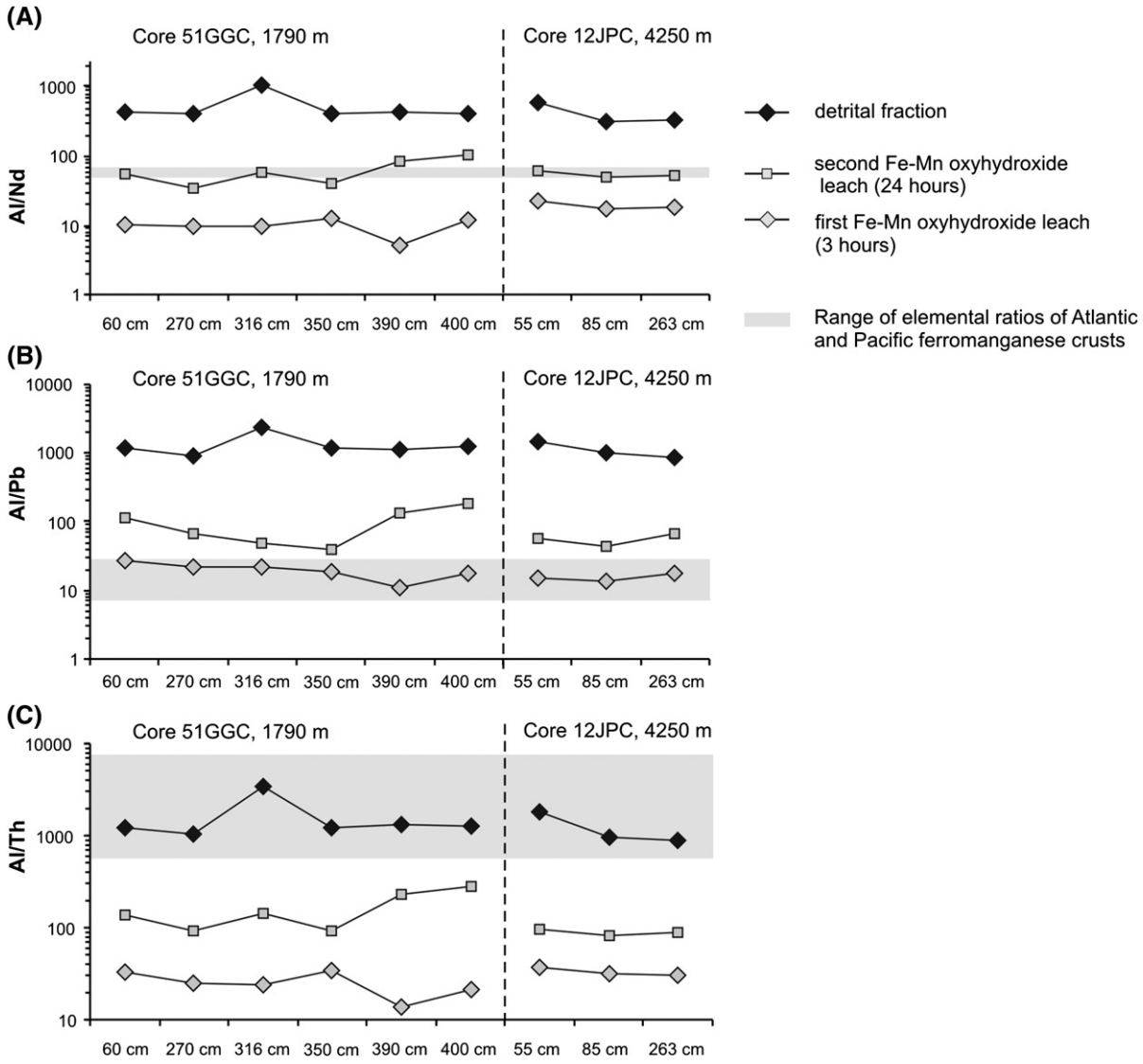

Fig. 5. Elemental ratios for three different chemical phases of the samples presented. Al/Nd for the leached coatings that were used for the isotope analyses (light grey diamonds) average 13 and are lower than hydrogenetic ferromanganese crusts in the equatorial Central and South Pacific (see also Table 5). Al/Pb of the first Fe–Mn oxyhydroxide fraction are similar to Pacific ferromanganese crust data, and Al/Th are orders of magnitude lower than ferromanganese crust data. This is, however, due to the absence of dissolved Th in the equatorial Central and South Pacific. Note the log scale of the *y*-axis. The individual elemental ratios are also displayed in Table 5. The gray boxes highlight the range of ferromanganese crust elemental ratios shown in Table 5.

apatite. Contrary to that, Haley et al. (2004) found no unambiguous indication that the MREE enrichment in porewaters containing dissolved phosphate is controlled by phosphates such as authigenic apatite. We cannot fully rule out that part of the REE signal extracted during leaching of the Fe–Mn oxyhydroxide fraction could be derived from contemporaneous leaching of authigenic apatite, but because of the preceding carbonate removal step this seems unlikely: Authigenic apatite can be easily dissolved using dilute acetic acid (Ohr et al., 1994), and the very first chemical reagent used here for the extraction of the carbonate fraction, preceding the reductive leaching of Fe–Mn oxyhydroxides, is an Na acetate buffer containing acetic acid (Fig. 1). Therefore, we attribute the MREE-enriched patterns shown in Fig. 4A, b to the release of REE from Fe–Mn oxyhydroxide coatings.

4.2. Mass balance calculations

Neodymium and Pb are highly enriched in the Fe–Mn oxyhydroxide fraction of marine sediments compared with the detrital fraction. These elements should thus be less prone to isotopic disturbance by detrital contamination than Sr. In order to constrain the reliability of the extracted $^{87}Sr/^{86}Sr$ as well as the $^{187}Os/^{188}Os$ signal as an indicator of detrital contamination of the extracted Nd and Pb signatures, we conducted a mass balance test using the elemental and isotopic distributions of Sr, Nd and Pb in the leached Fe–Mn oxyhydroxide coatings and the corresponding detrital fractions.

For the sediment samples the concentrations of Sr, Nd and Pb were measured in both the detrital and the two Fe–Mn oxyhydroxide coating fractions. The Sr isotope composition was determined for the first Fe–Mn oxyhydroxide and the detrital fraction. For simplicity, the second Fe–Mn oxyhydroxide leach and the residual detrital phase are considered together as the detrital phase because this second extracted phase represents a mixture of the authigenic and the detrital fraction, and the contribution to which cannot be further quantified here. The error introduced into the calculations by considering the second Fe–Mn oxyhydroxide fraction as part of the detrital fraction is considered a conservative buffer because it shifts the individual elemental mass balances towards the detrital fraction. In other words: Detrital contributions to the first extracted authigenic Fe–Mn oxyhydroxide fraction should become even more pronounced, which will be shown to have an insignificant effect for the extracted authigenic Nd and Pb isotope compositions (see below). The present-day seawater $^{87}Sr/^{86}Sr$ of 0.70918 is used as a reference to determine the detrital contribution f to the Fe–Mn oxyhydroxide leach:

$$f = \frac{\left(^{87}Sr/^{86}Sr_{mix} - {}^{87}Sr/^{86}Sr_{seawater}\right)}{\left(^{87}Sr/^{86}Sr_{detr} - {}^{87}Sr/^{86}Sr_{seawater}\right)}. \quad (1)$$

In Eq. (1), $^{87}Sr/^{86}Sr_{mix}$ represents the measured Sr isotope composition of the first Fe–Mn oxyhydroxide fraction. The total detrital Sr contribution to the first Fe–Mn oxyhydroxide fraction (in ng) is calculated as:

$$[Sr]_{detr,coating} = f \times [Sr]_{coating,total}. \quad (2)$$

The percentage p of Sr leached from the detrital fraction is then determined as

$$p = \left[\frac{[Sr]_{detr,coating}}{\left([Sr]_{detrital} + [Sr]_{detr,coating}\right)}\right] \times 100 \quad (3)$$

where p represents the total amount of leached detrital Sr (in %), $[Sr]_{detr,\ coating}$ is the amount of leached detrital Sr in the coating fraction and $[Sr]_{detrital}$ is the total mass of Sr present in the sample. Assuming that the same percentage of Nd and Pb was leached from the detrital fraction as for Sr, the total detrital Nd and Pb pools can be quantified:

$$[Nd, Pb]_{detr,total} = [Nd, Pb]_{detrital} \times \frac{100}{(100 - p)} \quad (4)$$

and the amount of Nd and Pb leached from the detrital fraction be calculated:

$$[Nd, Pb]_{detr,coating} = p \times [Nd, Pb]_{detr,total}. \quad (5)$$

$[Nd,\ Pb]_{detr,\ coating}$ refers to the amount of leached detrital Nd or Pb in the coating fraction. Following the quantification of the seawater contribution to the Nd and Pb Fe–Mn oxyhydroxide fraction (i.e., $[Nd, Pb]_{SW,\ coating}$)

$$[Nd, Pb]_{SW,coating} = [Nd, Pb]_{coating,total} - [Nd, Pb]_{detr,coating} \quad (6)$$

the hypothetical true seawater Nd and Pb isotope composition R can be determined:

$$R_{SW} = \frac{(R_{mix} - g \times R_{detritus})}{(1 - g)}. \quad (7)$$

$R = \varepsilon_{Nd}$, $^{206}Pb/^{204}Pb$, $^{207}Pb/^{204}Pb$, $^{208}Pb/^{204}Pb$, $^{207}Pb/^{206}Pb$, $^{208}Pb/^{206}Pb$. The variable g stands for the detrital contribution to the respective isotope signal (see below). In this case the seawater R was calculated as:

$$R_{SW} = \frac{\left(R_{mix} - \frac{[Nd,Pb]_{detr,coating}}{[Nd,Pb]_{coating,total}} \times R_{detritus}\right)}{\left(\frac{[Nd,Pb]_{SW,coating}}{[Nd,Pb]_{coating,total}}\right)}. \quad (8)$$

Table 6
Measured Sr, Nd and Pb concentrations, isotope ratios, and individual results of the mass balance calculations

Sample #	$^{87}Sr/^{86}Sr$	Sr [ng/g]	Nd [ng/g]	Pb [ng/g]	f (Eq. (1))	$Sr_{detr,\ coating}$ [ng/g] (Eq. (2))	p (Eq. (3))	$Nd_{detr,\ total}$ [ng/g] (Eq. (4))	$Nd_{detr,\ coating}$ [ng/g] (Eq. (5))	$Nd_{SW,\ coating}$ [ng/g] (Eq. (6))	$Pb_{detr,\ total}$ [ng/g] (Eq. (4))	$Pb_{detr,\ coating}$ [ng/g] (Eq. (5))	$Pb_{SW,\ coating}$ [ng/g] (Eq. (6))
Core 51GGC													
60 cm	0.70918	14,059	3515	1366	0.00011	2	0.003%	17,301	0.5	3515	6413	0.2	1366
60 cm detrital	0.72076	58,259	17,300	6412									
270 cm	0.70958	2451	4946	2183	0.03019	74	0.085%	26,653	22.7	4923	11,900	10.1	2173
270 cm detrital	0.72228	86,659	26,630	11890									
316 cm	0.70949	1083	2495	1140	0.02588	28	0.086%	5979	5.2	2490	2704	2.3	1138
316 cm detrital	0.72108	32,383	5973	2701									
350 cm	0.70977	2181	3895	2630	0.03404	74	0.075%	27,374	20.6	3874	9410	7.1	2623
350 cm detrital	0.72659	98,689	27,354	9403									
400 cm	0.70983	1130	2642	1786	0.04715	53	0.054%	24,117	13.1	2629	8049	4.4	1782
400 cm detrital	0.72307	98,200	24,104	8045									
Core 12JPC													
55 cm	0.71500	1368	4189	6346	0.29973	410	0.301%	24,905	74.8	4115	10,035	30.1	6316
55 cm detrital	0.72861	135,697	24,830	10,005									
85 cm	0.71391	1121	4684	6120	0.22109	248	0.159%	40,885	64.9	4619	12,809	20.3	6099
85 cm detrital	0.73057	155,606	40,821	12,788									
263 cm	0.71239	870	4248	4317	0.14025	122	0.083%	39,499	32.8	4215	15,426	12.8	4304
263 cm detrital	0.73207	146,781	39,466	15,413									

Sample #	Measured ε_{Nd} (detrital)	Measured ε_{Nd} (mix)	Calculated ε_{Nd} (seawater) (Eq. (8))	Δ sw–mix	Measured $^{206}Pb/^{204}Pb$ (detrital)	Measured $^{206}Pb/^{204}Pb$ (mix)	Calculated $^{206}Pb/^{204}Pb$ (seawater) (Eq. (8))	Δ sw–mix	Measured $^{207}Pb/^{204}Pb$ (detrital)	Measured $^{207}Pb/^{204}Pb$ (mix)	Calculated $^{207}Pb/^{204}Pb$ (seawater) (Eq. (8))	Δ sw–mix
Core 51GGC												
60 cm	−10.97	−9.97	−9.97	0.0001	18.992	19.134	19.134	0.0000	15.650	15.691	15.691	0.0000
270 cm	−10.83	−10.22	−10.22	0.0028	19.019	19.219	19.220	0.0009	15.649	15.684	15.685	0.0002
316 cm	−11.33	−10.32	−10.32	0.0021	18.882	19.123	19.123	0.0005	15.625	15.678	15.678	0.0001
350 cm	−12.39	−10.72	−10.71	0.0089	18.944	19.072	19.073	0.0003	15.625	15.667	15.667	0.0001
400 cm	−11.81	−9.44	−9.43	0.0118	19.101	18.980	18.980	−0.0003	15.636	15.662	15.662	0.0001
Core 12JPC												
55 cm	−15.02	−13.17	−13.14	0.0336	18.32	19.377	19.382	0.0051	15.527	15.693	15.694	0.0008
85 cm	−13.56	−11.10	−11.06	0.0346	18.69	19.112	19.113	0.0014	15.589	15.665	15.665	0.0003
263 cm	−12.21	−10.11	−10.10	0.0163	18.87	18.944	18.944	0.0002	15.625	15.654	15.654	0.0001

Sample #	Measured $^{208}Pb/^{204}Pb$ (detrital)	Measured $^{208}Pb/^{204}Pb$ (mix)	Calculated $^{208}Pb/^{204}Pb$ (seawater) (Eq. (8))	Δ sw–mix	Measured $^{207}Pb/^{206}Pb$ (detrital)	Measured $^{207}Pb/^{206}Pb$ (mix)	Calculated $^{207}Pb/^{206}Pb$ (seawater) (Eq. (8))	Δ sw–mix	Measured $^{208}Pb/^{206}Pb$ (detrital)	Measured $^{208}Pb/^{206}Pb$ (mix)	Calculated $^{208}Pb/^{206}Pb$ (seawater) (Eq. (8))	Δ sw–mix
Core 51GGC												
60 cm	38.886	39.162	39.162	0.0000	0.8240	0.8201	0.8201	0.00000	2.0475	2.0468	2.0468	0.00000
270 cm	38.902	39.274	39.275	0.0017	0.8228	0.8161	0.8161	−0.00003	2.0455	2.0435	2.0435	−0.00001
316 cm	38.739	39.131	39.131	0.0008	0.8275	0.8199	0.8199	−0.00002	2.0516	2.0463	2.0463	−0.00001
350 cm	38.874	39.076	39.076	0.0005	0.8248	0.8215	0.8215	−0.00001	2.0521	2.0488	2.0488	−0.00001
400 cm	38.969	38.898	38.897	−0.0002	0.8186	0.8252	0.8252	0.00002	2.0401	2.0494	2.0494	0.00002
Core 12JPC												
55 cm	38.522	39.591	39.596	0.0051	0.8477	0.8099	0.8097	−0.00018	2.1033	2.0432	2.0429	−0.00029
85 cm	38.804	39.173	39.174	0.0012	0.8340	0.8197	0.8196	−0.00005	2.0759	2.0497	2.0496	−0.00009
263 cm	38.935	38.921	38.921	0.0000	0.8281	0.8264	0.8264	−0.00001	2.0635	2.0545	2.0545	−0.00003

Equation numbers in brackets refer to equation numbers presented in the text. Large Delta refers to the difference between the calculated and the measured seawater isotope compositions.

Table 6 summarises the results for the individual calculations. The results of these mass balance calculations provide compelling evidence that the $^{87}Sr/^{86}Sr$ signal of the Fe–Mn oxyhydroxide fraction does not yield reliable information on the seawater origin of the measured Nd and Pb isotope signal. Not a single calculated seawater Nd and Pb isotope composition listed in Table 6 differs significantly from the measured Fe–Mn oxyhydroxide composition. For Nd the calculated offset from the true seawater signal is always significantly smaller than the analytical 2σ uncertainty of ± 0.27 ε_{Nd}. Indeed, even for the highest measured $^{87}Sr/^{86}Sr$, the offset of the calculated Nd seawater composition is an order of magnitude smaller than the external reproducibility (sample JPC12 — 55 cm, $^{87}Sr/^{86}Sr = 0.71500$; Table 6). A similar situation is observed for the Pb isotope signal. The offset of the calculated true seawater signal is always on the order of or smaller than the external reproducibility. Because of the large variability observed for the seawater Pb isotope signal on glacial–interglacial timescales, this renders the Pb isotope signal even more reliable than the Nd isotope signal. These calculations clearly imply that the present-day seawater $^{87}Sr/^{86}Sr$ can very well serve as proof for the seawater origin of the extracted Fe–Mn oxyhydroxide phase, such as shown for sites in the Cape Basin (cf., Piotrowski et al., 2005), but it cannot serve to disprove the seawater origin of the extracted Nd and Pb fraction.

The robustness of the extracted Fe–Mn oxyhydroxide Nd and Pb isotope signals can be tested further for hypothetical extreme Nd and Pb isotope composition of the detrital fraction. Fig. 6A illustrates the effect of altering the Nd isotope composition of the detrital fraction in the sediment. Even for unrealistically low $\varepsilon_{Nd,\ detritus}$ of -25 and a measured $^{87}Sr/^{86}Sr$ of 0.71209, the calculated seawater ε_{Nd} is offset from the measured value only by -0.10 ε_{Nd} units. In every case presented in Fig. 6A the offset of the calculated ε_{Nd} from the measured ε_{Nd} was significantly smaller than the long-term analytical external reproducibility of ± 0.27 ε_{Nd}. Equally consistent calculated seawater Pb isotope

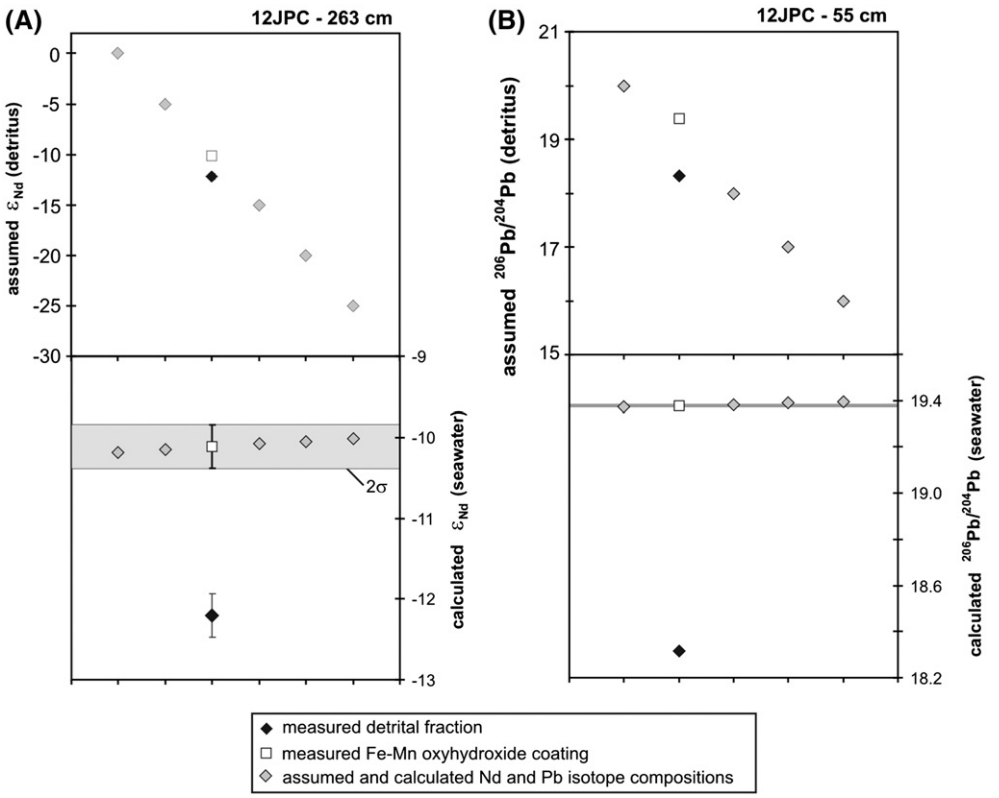

Fig. 6. (A) Calculated true ε_{Nd} for the extracted Fe–Mn oxyhydroxide fraction (lower panel), assuming a variety of possible detrital Nd isotope compositions (upper panel). Even detrital ε_{Nd} as low as -25 and as high as 0 do not change the calculated true seawater ε_{Nd} beyond the external reproducibility of 0.27 ε_{Nd}. (B) Calculated true $^{206}Pb/^{204}Pb$ for the extracted Fe–Mn oxyhydroxide fraction (lower panel), assuming a variety of possible complementary detrital $^{206}Pb/^{204}Pb$ isotope compositions (upper panel). Even detrital ε_{Nd} as low as 16.0 does not change the calculated true seawater $^{206}Pb/^{204}Pb$ to any significant extent.

compositions are found when modifying the detrital Pb isotope composition. In Fig. 6B the Pb isotopic behaviour is illustrated for $^{206}Pb/^{204}Pb$. Changing the $^{206}Pb/^{204}Pb$ of the detrital phase to ratios as low as 16.0 modifies the calculated seawater Pb isotope composition insignificantly (Fig. 6B). The other Pb isotope ratios provide identical information and are not displayed.

4.3. Thorium isotopes in Fe–Mn oxyhydroxide coatings

Due to the particle reactivity of Th, $^{232}Th/^{230}Th$ should be low in seawater-derived Fe–Mn oxyhydroxide coatings, as ^{232}Th can only be supplied to the oceans via continental input and is quickly removed at ocean margins (Guo et al., 1995; Swarzenski et al., 2003), whereas ^{230}Th is continuously produced in the water column through the decay of ^{238}U and ^{234}U. Uranium behaves conservatively in seawater under oxic conditions with a residence time of several 100 kyr, which is the reason why the production rate of ^{230}Th is homogeneous in all ocean basins (Nozaki, 1991; Dunk et al., 2002). Earlier studies demonstrated a systematic change in $^{232}Th/^{230}Th$ from proximal continental to distal marine environments (Guo et al., 1995; Robinson et al., 2004). Robinson et al. (2004) presented seawater $^{232}Th/^{230}Th$ in the range of 13,000 to 31,600 in depths between the surface and 1650 m water depth in both waters and carbonates close to the Bahamas. Although this location is relatively close to the Blake Ridge, it is isolated from direct continental influences because of the prevailing circulation regime (Anselmetti et al., 2000). The $^{232}Th/^{230}Th$ presented here are higher than the seawater $^{232}Th/^{230}Th$ presented by Robinson et al. (2004). However, considering the proximity of the Blake Ridge to the continental rise of eastern North America, the Holocene $^{232}Th/^{230}Th$ compositions seem to reflect a pure hydrogenetic signal, unaffected by detrital contributions. On the other hand, the ratios are significantly higher during the LGM and the deglaciation. The reasons for this can be twofold: Either sediment deposited during this interval was more prone to contemporaneous leaching of detrital Th, or the $^{232}Th/^{230}Th$ isotope composition along the Blake Ridge varied during the transition from the LGM to the Holocene.

It seems unlikely that partial leaching of the detrital phase is the cause for the higher ratios of Fe–Mn oxyhydroxide fractions older than the Holocene. In Fig. 5 Al/Th remains systematically low independent of the age of the sediment. Guo et al. (1995) published dissolved and particulate Th isotope compositions from waters offshore Cape Hatteras to the North of the Blake Ridge, ranging from 122,000 in surface water samples to 28,000 in 750 m water depth for dissolved $^{232}Th/^{230}Th$. Particulate $^{232}Th/^{230}Th$ was significantly higher, ranging from 231,000 to 143,000 in the same depth range.

Analogous to Nd and Pb, Th concentrations of the different sediment fractions shown in Table 5 indicate that a significant amount of bulk Th is locked in the seawater-derived fraction in sediments along the Blake Ridge, hence the differences in Al/Th between the three different fractions displayed in Table 5 and Fig. 5 are even more extreme than for Al/Nd and Al/Pb. The systematic variation between the two sequentially leached Fe–Mn oxyhydroxide fractions and the detrital fraction, which are independent of the age and the depth of the sediment cores, strongly suggests that the observed Th isotope signal is of seawater origin. The observation that $^{234}Th/^{232}Th$ in unfiltered water and particles are similar (Swarzenski et al., 2003) supports the notion that Th isotopes are not fractionated during incorporation into Fe–Mn oxyhydroxide coatings.

The amplitude of variation observed in $^{232}Th/^{230}Th$ between the LGM and the Holocene is not surprising considering the very short Th residence time in seawater. The residence time of dissolved ^{230}Th is on the order of <4 years in ocean margin settings and as long as 40 years in central ocean deep waters (Anderson et al., 1983b,a; Guo et al., 1995), which makes short-term seawater $^{232}Th/^{230}Th$ isotope variations very likely. The highest $^{232}Th/^{230}Th$ in core 51GGC was recorded at about 17.2 ka BP, immediately after the LGM. Considering the age uncertainties associated with radiocarbon dating during the deglaciation (Stuiver et al., 1998; Hughen et al., 2004) and the error induced by the uncertainty of the lock-in depth of the authigenic Fe–Mn oxyhydroxide signal (*i.e.* depth in the sediment below which the authigenic Fe–Mn oxyhydroxide is not modified anymore), the $^{232}Th/^{230}Th$ may have recorded the highly elevated IRD particle flux in the North Atlantic associated the large scale iceberg discharge event Heinrich 1 (~16.8 ka BP; Hemming, 2004).

4.4. Neodymium and lead mass balance

The reason for the consistency of the extracted Nd and Pb isotope signal in the mass balance calculations can best be illustrated by determining the induced offset from seawater compositions by the admixture of a detrital Sr, Nd and Pb. Knowing the total amount of seawater-derived Sr, Nd and Pb from Eq. (6), as well as the concentrations and the isotope compositions of the respective fractions, the imprint of detrital contamination to the seawater isotope signal can be determined. This is shown in Fig. 7, which highlights the susceptibility of the Sr isotope signal of the Fe–Mn oxyhydroxide fraction to

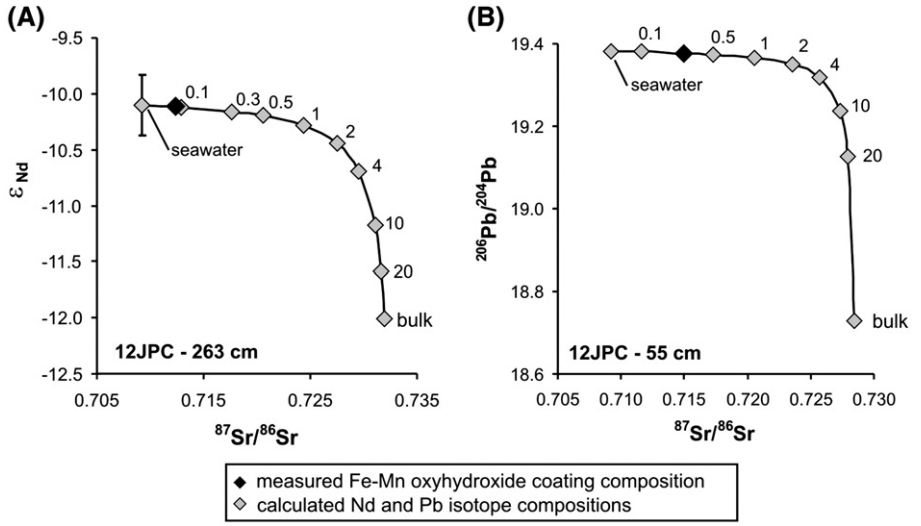

Fig. 7. (A) Measured and calculated ε_{Nd} for the extracted Fe–Mn oxyhydroxide fraction with increasing contemporaneous leaching of the detrital phase, exemplified for sample 12JPC — 263 cm. Numbers refer to the percentage of the detrital fraction that is extracted together with the Fe–Mn oxyhydroxide fraction. The figure demonstrates why even contributions as low as 0.1% of the detrital fraction already significantly disturb the Sr isotope composition while having no effect on the Nd isotope composition. (B) Measured and calculated $^{206}Pb/^{204}Pb$ for the extracted Fe–Mn oxyhydroxide fraction analogous to A, shown for sample 12JPC — 55 cm. Similar to the Nd isotope composition of the Fe–Mn oxyhydroxide fraction, the Pb isotope composition is very robust against detrital contamination of the Pb isotope system. The remaining Pb isotope compositions follow identical detrital phase admixing paths, which is why they are not shown here.

detrital contamination, accompanied by only insignificant offsets for the extracted Nd and Pb signal of the same fraction. The numbers along the mixing curve in Fig. 7 refer to the percentage of the detrital fraction that is extracted together with the Fe–Mn oxyhydroxide pool.

Even if 1% of the entire detrital fraction was extracted with the seawater-derived fraction, for mass balance constraints the Nd and Pb isotope signal would still be dominated by the Fe–Mn oxyhydroxide pool. In fact, all of the sediment samples processed for the mass balance calculation have 0.3% or less detrital contribution (*p* in Table 6).

5. Conclusions

The seawater-derived Fe–Mn oxyhydroxide fraction, extracted from marine drift sediments in the North Atlantic, is characterised by means of geochemical, radiogenic isotopic, and mass balance approaches to constrain the purity of the recorded seawater signal. Although the Sr and Os isotope compositions of the leached Fe–Mn oxyhydroxide fractions suggest contributions from the detrital pool in the sediments for these elements, this contribution is insignificant for Nd, Pb and Th isotopes due to mass balance constraints.

Thorium isotopes show a marked variation on glacial–interglacial timescales. Our data suggest that the seawater $^{232}Th/^{230}Th$ dropped significantly during the transition from the LGM to the Holocene. The high $^{232}Th/^{230}Th$ might be attributable to an increased particle load of the water masses in the western North Atlantic during the LGM, Heinrich 1 and the early deglaciation.

Al/Nd, Al/Pb and Al/Th ratios reveal a strong preferential enrichment of the trace metals relative to Al in the leached Fe–Mn oxyhydroxide phase compared with the detrital fraction. These elemental ratios are on the order of or lower than those for abyssal ferromanganese crusts from the central and South Pacific. The large difference in Al/Nd, Al/Pb and Al/Th ratios between the Fe–Mn oxyhydroxide fraction and the residual detrital fraction reflects the hydrogenous origin of the leached Fe–Mn oxyhydroxides.

The Fe–Mn oxyhydroxide fraction that was extracted from marine drift sediments through reductive leaching displays REE patterns virtually identical to Fe-rich anoxic marine pore waters, in which the dissolved trace metals are ultimately of seawater orgin. The observed MREE enrichment is controlled by REE released from Fe–Mn oxyhydroxides.

The mass balance calculations demonstrate that the Nd and Pb isotope signature of the leached Fe–Mn oxyhydroxide fraction is not sensitive to detrital contamination, even for extremely elevated $^{87}Sr/^{86}Sr$ or unrealistically low detrital ε_{Nd}. This observation is ascribed to the strong enrichment of Nd and Pb in the authigenic fraction of the sediments.

Elemental ratios such as Al/Nd, Al/Pb or Al/Th, as well as REE patterns contain valuable information regarding the assessment of whether the extracted authigenic Fe–Mn oxyhydroxide fraction was contaminated through detrital contributions. Carrying out these tests for drift sediments along the Blake Ridge confirmed that a pure seawater component for Nd and Pb can be extracted. This applies to marine sediments analysed from this specific location. Although we expect sediments in different locations in the oceans to show similar trace metal distributions, this has to be confirmed on a site-specific basis. Possible contributions of pre-formed riverine Fe–Mn oxyhydroxide coatings that might be present in some proximal continental margin settings cannot be unambiguously identified with the methods applied here and have to be critically evaluated by other methods at these locations.

Acknowledgments

M. B. Andersen, E.-K. Potter and M. Wipf are acknowledged for providing assistance with the Th separation and measurements. Dieter Garbe-Schönberg at the Geological Institute of the University of Kiel carried out the major and trace element ICP-AES and ICP-MS measurements. Brian Haley and Sidney Hemming provided additional constructive suggestions. Derek Vance and an anonymous reviewer improved an earlier version of the manuscript by providing additional constructive suggestions. Lynn Walter and D. Rickards are thanked for editorial handling.

References

Alleman, L.Y., Veron, A.J., Church, T.M., Flegal, A.R., Hamelin, B., 1999. Invasion of the abyssal North Atlantic by modern anthropogenic lead. Geophysical Research Letters 26 (10), 1477–1480.

Andersen, M.B., Stirling, C.H., Potter, E.K., Halliday, A.N., 2004. Toward epsilon levels of measurement precision on U-234/U-238 by using MC-ICPMS. International Journal of Mass Spectrometry 237 (2–3), 107–118.

Anderson, R.F., Bacon, M.P., Brewer, P.G., 1983a. Removal of 230Th and 231Pa at ocean margins. Earth and Planetary Science Letters 66, 73–90.

Anderson, R.F., Bacon, M.P., Brewer, P.G., 1983b. Removal of 230Th and 231Pa from the open ocean. Earth and Planetary Science Letters 62 (1), 7–23.

Anselmetti, F.S., Eberli, G.P., Ding, Z.D., 2000. From the Great Bahama Bank into the Straits of Florida: a margin architecture controlled by sea-level fluctuations and ocean currents. Geological Society of America Bulletin 112 (6), 829–844.

Bayon, G., German, C.R., Boella, R.M., Milton, J.A., Taylor, R.N., Nesbitt, R.W., 2002. An improved method for extracting marine sediment fractions and its application to Sr and Nd isotopic analysis. Chemical Geology 187 (3–4), 179–199.

Bayon, G., German, C.R., Burton, K.W., Nesbitt, R.W., Rogers, N., 2004. Sedimentary Fe–Mn oxyhydroxides as paleoceanographic archives and the role of aeolian flux in regulating oceanic dissolved REE. Earth and Planetary Science Letters 224 (3–4), 477–492.

Belshaw, N.S., Freedman, P.A., O'Nions, R.K., Frank, M., Guo, Y., 1998. A new variable dispersion double-focusing plasma mass spectrometer with performance illustrated for Pb isotopes. International Journal of Mass Spectrometry 181, 51–58.

Birck, J.L., Barman, M.R., Capmas, F., 1997. Re–Os isotopic measurements at the femtomole level in natural samples. Geostandards Newsletter 21 (1), 19–27.

Biscaye, P.E., Anderson, R.F., Deck, B.L., 1988. Fluxes of particles and constituents to the eastern United States continental slope and rise — Seep-I. Continental Shelf Research 8 (5–7), 855–904.

Boyle, E.A., Keigwin, L.D., 1985. Comparison of Atlantic and Pacific paleochemical records for the last 215,000 years — changes in deep ocean circulation and chemical inventories. Earth and Planetary Science Letters 76 (1–2), 135–150.

Chester, R., Hughes, M.J., 1967. A chemical technique for the separation of ferromanganese minerals, carbonate minerals and adsorbed trace elements for pelagic sediments. Chemical Geology 2, 249–262.

Cohen, A.S., Onions, R.K., Siegenthaler, R., Griffin, W.L., 1988. Chronology of the pressure–temperature history recorded by a granulite terrain. Contributions to Mineralogy and Petrology 98 (3), 303–311.

Creaser, R.A., Papanastassiou, D.A., Wasserburg, G.J., 1991. Negative thermal ion mass-spectrometry of osmium, rhenium, and iridium. Geochimica et Cosmochimica Acta 55 (1), 397–401.

Dunk, R.M., Mills, R.A., Jenkins, W.J., 2002. A reevaluation of the oceanic uranium budget for the Holocene. Chemical Geology 190 (1–4), 45–67.

Eittreim, S., Ewing, M., Thorndik, E.M., 1969. Suspended matter along continental margin of North American basin. Deep-Sea Research 16 (6), 613–624.

Eittreim, S., Thorndike, E.M., Sullivan, L., 1976. Turbidity distribution in Atlantic Ocean. Deep-Sea Research 23 (12), 1115–1127.

Elderfield, H., Sholkovitz, E.R., 1987. Rare earth elements in the pore waters of reducing nearshore sediments. Earth and Planetary Science Letters 82 (3–4), 280–288.

Foster, G.L., Vance, D., 2006. Negligible glacial–interglacial variation in continental chemical weathering rates. Nature 444 (7121), 918–921.

Frank, M., 2002. Radiogenic isotopes: tracers of past ocean circulation and erosional input. Reviews of Geophysics 40 (1) (Article No.: 1001).

Galer, S.J.G., Abouchami, W., 1998. Practical application of lead triple spiking for correction of instrumental mass discrimination. Mineralogical Magazine 62A, 491–492.

Goldstein, S.L., Hemming, S.R., 2003. Long-lived isotopic tracers in oceanography, paleoceanography, and ice-sheet dynamics. Treatise on Geochemistry 6, 453–489.

Guo, L.D., Santschi, P.H., Baskaran, M., Zindler, A., 1995. Distribution of dissolved and particulate Th-230 and Th-232 in seawater from the Gulf of Mexico and off Cape Hatteras as measured by SIMS. Earth and Planetary Science Letters 133 (1–2), 117–128.

Haley, B.A., Klinkhammer, G.P., McManus, J., 2004. Rare earth elements in pore waters of marine sediments. Geochimica et Cosmochimica Acta 68 (6), 1265–1279.

Hannigan, R.E., Sholkovitz, E.R., 2001. The development of middle rare earth element enrichments in freshwaters: weathering of phosphate minerals. Chemical Geology 175 (3–4), 495–508.

Hein, J.R., Koschinsky, A., Bau, M., Manheim, F.T., Kang, J.-K., Roberts, L., 1999. Cobalt-rich ferromanganese crusts in the Pacific. In: Cronan, D.S. (Ed.), Handbook of Marine Mineral Deposits. CRC Press, pp. 239–279.

Hemming, S.R., 2004. Heinrich events: massive late pleistocene detritus layers of the North Atlantic and their global climate imprint. Reviews of Geophysics 42 (1), RG1005.

Henderson, G.M., Maier-Reimer, E., 2002. Advection and removal of 210Pb and stable Pb isotopes in the oceans: a general circulation model study. Geochimica et Cosmochimica Acta 66 (2), 257–272.

Henderson, G.M., Martel, D.J., Onions, R.K., Shackleton, N.J., 1994. Evolution of seawater Sr-87/Sr-86 over the last 400 ka — the absence of glacial–interglacial cycles. Earth and Planetary Science Letters 128 (3–4), 643–651.

Horwitz, E.P., Chiarizia, R., Dietz, M.L., 1992. A novel strontium-selective extraction chromatographic resin. Solvent Extraction and Ion Exchange 10 (2), 313–336.

Hughen, K.A., Baillie, M.G.L., Bard, E., Beck, J.W., Bertrand, C.J.H., Blackwell, P.G., Buck, C.E., Burr, G.S., Cutler, K.B., Damon, P.E., Edwards, R.L., Fairbanks, R.G., Friedrich, M., Guilderson, T.P., Kromer, B., McCormac, G., Manning, S., Ramsey, C.B., Reimer, P.J., Reimer, R.W., Remmele, S., Southon, J.R., Stuiver, M., Talamo, S., Taylor, F.W., van der Plicht, J., Weyhenmeyer, C.E., 2004. Marine04 marine radiocarbon age calibration, 0–26 cal kyr BP. Radiocarbon 46, 1059–1086.

Jacobsen, S.B., Wasserburg, G.J., 1980. Sm–Nd isotopic evolution of chondrites. Earth and Planetary Science Letters 50 (1), 139–155.

Keigwin, L.D., 2004. Radiocarbon and stable isotope constraints on Last Glacial Maximum and Younger Dryas ventilation in the western North Atlantic. Paleoceanography 19 (4) (Article No.: PA4012).

Klemm, V., Levasseur, S., Frank, M., Hein, J.R., Halliday, A.N., 2005. Osmium isotope stratigraphy of a marine ferromanganese crust. Earth and Planetary Science Letters 238 (1–2), 42–48.

Levasseur, S., Birck, J.-L., Allègre, C.J., 1998. Direct measurement of femtomoles of osmium and the 187Os/186Os ratio in seawater. Science 282, 272–274.

Lugmair, G.W., Galer, S.J.G., 1992. Age and isotopic relationships among the angrites Lewis Cliff 86010 and Angra dos Reis. Geochimica et Cosmochimica Acta 56 (4), 1673–1694.

Luo, X.Z., Rehkamper, M., Lee, D.C., Halliday, A.N., 1997. High precision Th-230/Th-232 and U-234/U-238 measurements using energy-filtered ICP magnetic sector multiple collector mass spectrometry. International Journal of Mass Spectrometry 171 (1–3), 105–117.

McCave, I.N., 1986. Local and global aspects of the bottom nepheloid layers in the world ocean. Netherlands Journal of Sea Research 20 (2–3), 167–181.

McLennan, S.M., 1989. Rare earth elements in sedimentary rocks — influence of provenance and sedimentary processes. Reviews in Mineralogy 21, 169–200.

Nier, A.O., 1938. The isotopic constitution of strontium, barium, bismuth, thallium and mercury. Physical Review 54 (4), 275–278.

Nozaki, Y., 1991. The systematics and kinetics of U–Th decay series nuclides in ocean water. Reviews in Aquatic Sciences 4 (1), 75–105.

Ohr, M., Halliday, A.N., Peacor, D.R., 1994. Mobility and fractionation of rare earth elements in argillaceous sediments: implications for dating diagenesis and low-grade metamorphism. Geochimica et Cosmochimica Acta 58 (1), 289–312.

Palmer, M.R., Elderfield, H., 1985. Sr isotope composition of sea water over the past 75 Myr. Nature 314 (6011), 526–528.

Peucker-Ehrenbrink, B., Ravizza, G., 2000. The marine osmium isotope record. Terra Nova 12, 205–219.

Piotrowski, A.M., 2004. A high resolution record of ocean circulation during the Last Glacial Cycle from Neodymium isotopes. Thesis — Columbia University.

Piotrowski, A.M., Goldstein, S.L., Hemming, S.R., Fairbanks, R.G., 2004. Intensification and variability of ocean thermohaline circulation through the last deglaciation. Earth and Planetary Science Letters 225 (1–2), 205–220.

Piotrowski, A.M., Goldstein, S.L., Hemming, S.R., Fairbanks, R.G., 2005. Temporal relationships of carbon cycling and ocean circulation at glacial boundaries. Science 307 (5717), 1933–1938.

Rehkamper, M., Schonbachler, M., Stirling, C.H., 2001. Multiple collector ICP-MS: introduction to instrumentation, measurement techniques and analytical capabilities. Geostandards Newsletter— the Journal of Geostandards and Geoanalysis 25 (1), 23–40.

Robinson, L.F., Belshaw, N.S., Henderson, G.M., 2004. U and Th concentrations and isotope ratios in modern carbonates and waters from the Bahamas. Geochimica et Cosmochimica Acta 68 (8), 1777–1789.

Rutberg, R.L., Hemming, S.R., Goldstein, S.L., 2000. Reduced North Atlantic Deep Water flux to the glacial Southern Ocean inferred from neodymium isotope ratios. Nature 405 (6789), 935–938.

Ruttenberg, K.C., 1992. Development of a sequential extraction method for different forms of phosphorus in marine sediments. Limnology and Oceanography 37 (7), 1460–1482.

Schaule, B.K., Patterson, C.C., 1981. Lead concentrations in the northeast Pacific — evidence for global anthropogenic perturbations. Earth and Planetary Science Letters 54 (1), 97–116.

Steiger, R.H., Jager, E., 1977. Subcommission on geochronology: convention on the use of decay constants in geo- and cosmochronology. Earth and Planetary Science Letters 36 (3), 359–362.

Stuiver, M., Reimer, P.J., Bard, E., Beck, J.W., Burr, G.S., Hughen, K.A., Kromer, B., McCormac, G., Van der Plicht, J., Spurk, M., 1998. INTCAL98 radiocarbon age calibration, 24,000-0 cal BP. Radiocarbon 40 (3), 1041–1083.

Swarzenski, P.W., Porcelli, D., Andersson, P.S., Smoak, J.M., 2003. The behavior of U- and Th-series nuclides in the estuarine environment, uranium-series geochemistry. Reviews in Mineralogy and Geochemistry 577–606.

Tanaka, T., Togashi, S., Kamioka, H., Amakawa, H., Kagami, H., Hamamoto, T., Yuhara, M., Orihashi, Y., Yoneda, S., Shimizu, H., Kunimaru, T., Takahashi, K., Yanagi, T., Nakano, T., Fujimaki, H., Shinjo, R., Asahara, Y., Tanimizu, M., Dragusanu, C., 2000. JNdi-1: a neodymium isotopic reference in consistency with LaJolla neodymium. Chemical Geology 168 (3–4), 279–281.

Tessier, A., Campbell, P.G.C., Bisson, M., 1979. Sequential extraction procedure for the speciation of particulate trace metals. Analytical Chemistry 51 (7), 844–851.

Thirlwall, M.F., 2002. Multicollector ICP-MS analysis of Pb isotopes using a 207Pb–204 Pb double spike demonstrates up to 400 ppm/amu systematic errors in Tl-normalization. Chemical Geology 184 (3–4), 255–279.

Thomson, J., Higgs, N.C., Croudace, I.W., Colley, S., Hydes, D.J., 1993. Redox zonation of elements at an oxic/post-oxic boundary in deep-sea sediments. Geochimica et Cosmochimica Acta 57 (3), 579–595.

Thomson, J., Higgs, N.C., Wilson, T.R.S., Croudace, I.W., De Lange, G.J., Van Santvoort, P.J.M., 1995. Redistribution and geochemical behaviour of redox-sensitive elements around S1, the most recent eastern Mediterranean sapropel. Geochimica et Cosmochimica Acta 59 (17), 3487–3501.

Tovar-Sanchez, A., Sanudo-Wilhelmy, S.A., Garcia-Vargas, M., Weaver, R.S., Popels, L.C., Hutchins, D.A., 2003. A trace metal clean reagent to remove surface-bound iron from marine phytoplankton. Marine Chemistry 82 (1–2), 91–99.

van de Flierdt, T., Frank, M., Halliday, A.N., Hein, J.R., Hattendorf, B., Gunther, D., Kubik, P.W., 2003. Lead isotopes in North Pacific

deep water — implications for past changes in input sources and circulation patterns. Earth and Planetary Science Letters 209 (1–2), 149–164.

Volkening, J., Walczyk, T., Heumann, K.G., 1991. Osmium isotope ratio determinations by negative thermal ionization mass-spectrometry. International Journal of Mass Spectrometry and Ion Processes 105 (2), 147–159.

Walder, A.J., Furuta, N., 1993. High-precision lead-isotope ratio measurement by inductively-coupled plasma multiple collector mass-spectrometry. Analytical Sciences 9 (5), 675–680.